JOURNAL OF VIROLOGY, Apr. 2008, p. 3971–3983 Vol. 82, No. 8
0022-538X/08/$08.00+0 doi:10.1128/JVI.02592-07


# Mechanisms of Varicella-Zoster Virus Neuropathogenesis in Human Dorsal Root Ganglia[▽]

Mike Reichelt,* Leigh Zerboni, and Ann M. Arvin

*Departments of Pediatrics and Microbiology & Immunology, Stanford University School of Medicine, Stanford, California 94305*

Received 5 December 2007/Accepted 29 January 2008

**Varicella-zoster virus (VZV) is a human alphaherpesvirus that infects sensory ganglia and reactivates from latency to cause herpes zoster. VZV replication was examined in human dorsal root ganglion (DRG) xenografts in mice with severe combined immunodeficiency using multiscale correlative immunofluorescence and electron microscopy. These experiments showed the presence of VZV genomic DNA, viral proteins, and virion production in both neurons and satellite cells within DRG. Furthermore, the multiscale analysis of VZV-host cell interactions revealed virus-induced cell-cell fusion and polykaryon formation between neurons and satellite cells during VZV replication in DRG in vivo. Satellite cell infection and polykaryon formation in neuron-satellite cell complexes provide mechanisms to amplify VZV entry into neuronal cell bodies, which is necessary for VZV transfer to skin in the affected dermatome during herpes zoster. These mechanisms of VZV neuropathogenesis help to account for the often severe neurologic consequences of herpes zoster.**

Varicella-zoster virus (VZV) is a human neurotropic alphaherpesvirus with a linear DNA genome that has at least 70 open reading frames (ORFs) encoding viral proteins (4). VZV causes varicella during primary infection, establishes latency in sensory ganglia, and may reactivate to cause herpes zoster (4, 12). VZV persistence in cranial nerve and dorsal root sensory ganglia appears to be a consistent consequence of primary VZV infection (4, 5, 12, 31). VZV is related to herpes simplex virus types 1 and 2 (HSV-1 and -2), which are also neurotropic human alphaherpesviruses that establish latency in sensory ganglia, but in contrast to VZV, HSV reactivations are common and usually asymptomatic (30). When VZV reactivates, the characteristic dermatomal rash of herpes zoster is attributed to the axonal transport of VZ virions that were assembled in neuronal cell bodies to the skin. Clinically, herpes zoster is characterized by severe acute pain and a dermatomal rash and often by prolonged neurologic signs and symptoms (12).

Because VZV is a highly host-specific pathogen, we have used human tissue xenografts in mice with severe combined immunodeficiency (SCID) to analyze VZV tropisms for differentiated human cells in vivo (35). Autopsy studies provide some limited information about the acute VZV infection that occurs in sensory ganglia during reactivation. A marked disruption of cellular architecture within the ganglion, viral protein expression, and detection of herpesvirus-like particles have been reported (8, 14, 20, 23). Our dorsal root ganglion (DRG) model of neuropathogenesis makes it possible to examine the interactions between VZV and human neurons and satellite cells located within their typical tissue microenvironment (35, 36). In DRG xenografts, VZV inoculation results in viral DNA synthesis, expression of immediate-early (IE) regulatory/tegument proteins IE62 and IE63 and envelope glycoproteins, and the production of infectious virus.

The purpose of these experiments was to investigate VZV replication in human DRG using multiscale correlative immunofluorescence-electron microscopy (IF-EM) to analyze neurons and satellite cells over a wide range of resolutions and magnifications. Correlative IF-EM is being exploited in cell and developmental biology and neuroscience (7, 10, 11, 22) and has been used in a few investigations of viral pathogenesis (1, 21). Infected cells within the complex DRG tissues were identified by IF detection of viral proteins and VZV DNA, followed by EM and immuno-EM in ultrastructural analyses to localize viral DNA, nucleocapsids, and VZ virions in the same cell. These experiments provide new insights about how VZV interactions with neural cells in sensory ganglia result in the characteristic manifestations of herpes zoster.

## MATERIALS AND METHODS

**DRG xenotransplantation.** Human fetal DRG were inserted under the kidney capsule of male C.B-17$^{scid/scid}$ mice (Taconic Farms, Germantown, NY) (35). The Stanford University Administrative Panel on Laboratory Animal Care approved all animal protocols. Human tissues were provided by Advanced Bioscience Resources (ABR, Alameda, CA) and were obtained in accordance with state and federal regulations.

**Viruses and infection of DRG xenografts.** VZV (rOka) was propagated in human embryonic lung fibroblasts cells for inoculation of DRG xenografts; inoculum titers were determined by infectious focus assay at the time of injection (35). DRG were infected by direct injection of VZV-infected fibroblasts at 4 to 12 weeks after xenotransplantation (35). At designated times after inoculation, mice were euthanized and DRG were removed and immersed in 4% paraformaldehyde (PFA) in phosphate buffer (0.1 M, pH 7.2) on ice for immediate fixation.

**Preparation of DRG for standard EM.** DRG xenografts were fixed in 4% PFA and 2% glutaraldehyde in phosphate buffer (0.1 M, pH 7.2), postfixed with 1% osmium tetroxide, and incubated in 1% aqueous uranyl acetate overnight. The samples were dehydrated in a series of increasing ethanol concentrations followed by a final propylenoxide step. The samples were embedded in Embed812 (Electron Microscopy Sciences, Fort Washington, PA). Ultrathin sections (50 to 80 nm) were prepared with a diamond knife (Diatome) and an ultramicrotome (Ultracut; Leica). Sections were stained with 3.5% aqueous uranyl acetate for 5 min and with 0.2% lead citrate for 3 min. The sections were analyzed using a

* Corresponding author. Mailing address: Stanford University School of Medicine, 300 Pasteur Dr., Grant Bldg., Room S356, Stanford, CA 94305. Phone: (650) 723-6353. Fax: (650) 725-8040. E-mail: reichelt@stanford.edu.

▽ Published ahead of print on 6 February 2008.

JEOL 1230 transmission electron microscope (TEM) at 80 kV, and digital photographs were taken with a GATAN Multiscan 701 digital camera.

**Preparation of DRG for correlative IF-EM using LR-White resin.** DRG xenografts were fixed in 4% PFA and 0.1% glutaraldehyde in phosphate buffer (0.1 M, pH 7.2). The samples were dehydrated in a series of increasing ethanol concentrations and embedded in LR-White resin. Polymerization was at 50°C for 3 days. Ultrathin sections were prepared, stained, and analyzed as described for standard EM sections. LR-White sections were used for DNA in situ hybridization and immuno-EM.

For cryosectioning, DRG xenografts were fixed in 4% PFA with 0.1% glutaraldehyde in phosphate buffer (0.1 M, pH 7.2), washed several times in phosphate-buffered saline, and infiltrated in 2.3 M sucrose overnight at 4°C (32). Samples were mounted on pins for cryo-ultramicrotomy and frozen in liquid nitrogen. Semithin cryosections (500 nm) for IF analysis were prepared with a glass knife at −80°C, and ultrathin cryosections (80 nm) were prepared with a diamond knife (Diatome) at −130°C using an ultramicrotome (Ultracut, Leica) equipped with a cryosectioning chamber. Thawed cryosections were transferred to Formvar- and carbon-coated EM grids (nickel) in a drop of 2.3 M sucrose and stained for IF or counterstained for EM with 0.5% uranyl acetate in 2% methylcellulose for 10 min on ice.

**Immunolabeling of thawed cryosections and LR-White sections for IF and correlative IF-EM and immuno-EM.** Sections were blocked in digoxigenin (DIG) blocking solution (Roche) for 30 min. Primary antibodies were diluted in blocking solution and incubation was for 1 h at room temperature. Secondary fluorophore-conjugated antibodies or protein A-gold conjugates were diluted in blocking solution and sections were incubated for 1 h or 30 min, respectively. Samples for IF-EM analysis were first mounted in glycerol and after IF analysis were counterstained for EM as described above. The primary antibodies included rabbit polyclonal antibodies anti-IE62 (a gift from Paul Kinchington, University of Pittsburgh), anti-IE63 (a gift from William Ruyechan), anti-ORF47 (3), and anti-human synaptophysin (Zymed, South San Francisco, CA) and monoclonal antibodies anti-DIG (Roche), anti-NCAM (Zymed, South San Francisco, CA), and anti-gE (Chemicon, Temecula, CA). Antibodies and reagents used for secondary detection included goat anti-mouse–fluorescein isothiocyanate (FITC), goat anti-mouse–Alexa 488, rabbit anti-mouse–Alexa 488, anti-rabbit–FITC, anti-mouse–Texas red, and anti-rabbit–Texas red (Invitrogen/Molecular Probes). Protein A conjugated to 15-nm colloidal gold (PAG15 nm) was from CMC (Utrecht, The Netherlands). Hoechst 22358 was used as a nuclear counterstain.

**In situ hybridization for VZV genomic DNA detection in DRG by confocal IF and immuno-EM.** The VZV-specific DNA probe was prepared by random priming using the DIG DNA labeling kit (Roche Diagnostics, Penzberg, Germany) and a VZV genomic DNA HindIII-C fragment as a template. One milliliter of the hybridization mix contained 50% Formamide, 10% dextran sulfate, 1× SSC (1× SSC is 0.15 M NaCl plus 0.015 M sodium citrate), 1× Denhardt's solution, 0.5 mg salmon sperm DNA, and 0.01 ml DIG-labeled VZV DNA probe. The hybridization mix was heat denatured for 10 min at 95°C and chilled on ice. LR-White sections or thawed cryosections were denatured in 0.5 M NaOH for 5 min. After overnight hybridization at 37°C, sections were washed twice in 2× SSC and 0.1× SSC (twice for 15 min each) and then blocked in DIG blocking solution (Roche). Sections were incubated with anti-DIG monoclonal antibody (Roche) for 1 h. Secondary detection for immuno-EM was with rabbit anti-mouse antibody followed by PAG15 nm. For IF-EM, secondary detection was with rabbit anti-mouse–Alexa 488 antibody followed by PAG15 nm.

**Correlative IF-EM analysis.** Ultrathin sections were transferred to locator grids (Maxtaform, 200 mesh, nickel; Ted Pella). Combined IF and immunogold labeling was performed as described above. Confocal microscopy was done to evaluate the staining and to find areas of interest. The coordinates of the location of these areas were noted. After confocal analysis, the glycerol was washed off the grids with water and sections were counterstained for EM analysis. The areas of interest were then located and examined by TEM at low magnification using the coordinates and further investigated at higher magnification.

**Image processing and analysis.** Sections stained for IF analysis were imaged using a Leica TCS$^{SP2}$ confocal laser-scanning microscope (Heidelberg, Germany) and a ×63/1.4 Plan Apochromat. Images were scanned at 1,024 by 1,024 pixels, with 4× frame averaging and the pinhole adjusted to 1 Airy unit. Brightness and contrast were adjusted using Photoshop CS3 (Adobe). All images were captured under the same conditions within each type of experiment. The percentage of infected neuron-satellite cell complexes (NSC) with evidence of polykaryon formation was estimated by evaluation of NCAM staining of cell membranes and cytoplasmic staining of IE62 or IE63 from a total of 252 NSC. In the control experiments for VZV-induced polykaryon formation, neuronal cell adhesion molecule (NCAM) staining of approximately 50 NSC in different sections of one uninfected/unimplanted human DRG and 108 NSC (with 679 satellite cells) in different sections of one mock-infected/unimplanted human DRG was evaluated.

## RESULTS

**IE, early, and late VZV proteins are expressed in both neurons and satellite cells.** The precise cellular localization of viral proteins and viral genomic DNA within DRG requires a histological resolution that distinguishes the neuronal cell body from the surrounding satellite cells, which form a thin envelope around the neuron (15). To achieve this resolution and to identify infected cells, we used thin (500 nm) cryosections of infected DRG or uninfected control DRG stained with antibodies against the IE proteins IE62 and IE63 or the viral kinase early protein ORF47 (Fig. 1). Cell nuclei were counterstained with Hoechst 22358. Strong expression of IE62 and IE63 (Fig. 1a and b) as well as of ORF47 (Fig. 1c) was evident in nuclei of approximately 80% of cells in the NSC of acutely infected DRG. These complexes have a characteristic histological appearance, with a large neuronal cell body (>50 μm), a prominent neuron nucleus (10 to 20 μm) and the concentric arrangement of the satellite cells around the neuron (Fig. 1a, b, i, and k). Inspection of 250 NSC in multiple sections of two DRG revealed expression of IE62, IE63, and ORF47 proteins, as illustrated in Fig. 1a to c; in the prominent nuclei of neurons; and in the surrounding ring of smaller nuclei of satellite cells. These proteins were also detected in the cytoplasm of both neurons and satellite cells, but cytoplasmic expression was less intense. Envelope glycoproteins are required to produce infectious virus particles. Therefore, DRG sections were stained for glycoprotein E (gE), which is the most abundant late viral glycoprotein, (Fig. 1d). gE expression was most prominent at the cell boundaries of both neurons and satellite cells. The outer boundaries of satellite cells showed extensive gE staining (Fig. 1d), indicating that gE was expressed on regions of satellite cell plasma membranes that were not in direct contact with those of infected neurons. Uninfected DRG showed no evidence of nonspecific staining (Fig. 1a′ to d′).

**VZV genomic DNA is present in the nuclei of both neurons and satellite cells.** The expression of IE62, IE63, ORF47, and gE in neurons and satellite cells indicated that VZV genomic DNA was present in both cell types. VZV DNA synthesis was assessed using fluorescence DNA in situ hybridization with a DIG-labeled VZV-HindIII-C DNA probe, in combination with immunofluorescence for IE62 and nuclear Hoechst staining. As shown in representative images of an infected neuron with adjacent infected satellite cells, viral DNA was detected in the nucleus of the neuron and in the nuclei of the surrounding satellite cells that exhibited IE62 expression (Fig. 1f to h). Partial colocalization of the VZV DNA signal with IE62 within the nucleus was demonstrated in the merged image (Fig. 1h). The intensity of the VZV DNA signal in the nuclei of satellite cells and neurons that expressed IE62 varied from weak, as shown in the satellite cell labeled "s1," to strong, as illustrated by the satellite cell labeled "s2′ and the neuron. No background VZV DNA signal was detected in uninfected DRG (Fig. 1e).

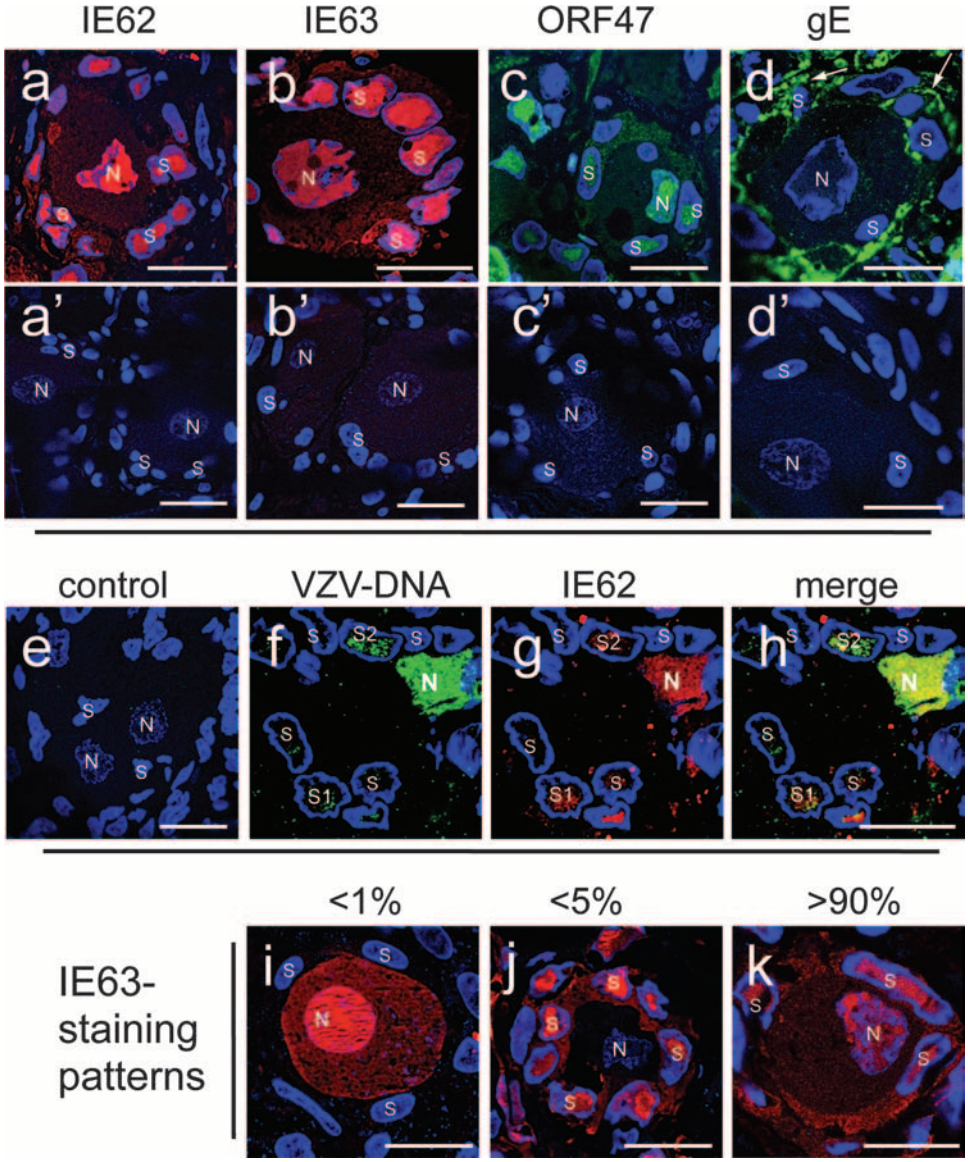


FIG. 1. VZV IE and late proteins and viral DNA are detected in neurons and satellite cells of acutely infected DRG. Cryosections of acutely infected DRG were stained for IE62 (a and g; red), IE63 (b and i to k; red), ORF47 (c; green), or gE (d, green). Primary antibodies were detected with Texas red-labeled goat anti-rabbit antibody (IE62 and IE63), FITC-labeled goat anti-rabbit antibody (ORF47), or FITC-labeled goat anti-mouse antibody (gE). VZV genomic DNA was detected by DNA in situ hybridization (e, f, and h; green) with a DIG-labeled HindIII-C VZV DNA probe and staining with a mouse monoclonal anti-DIG antibody and FITC-labeled goat anti-mouse antibody. Panel h shows the merge of VZV DNA staining (green) and IE62 labeling (red). Control staining of uninfected tissue with the corresponding antibody combinations or DNA probe is shown in panels a′ to d′ and e, respectively. The nuclear DNA was counterstained with Hoechst 22358 (blue). Distinct patterns of IE63 (red) staining and their approximate abundance as the percentage of 100 NSC are shown in panels i to k. Nuclei of neurons (N) and satellite cells (s) are marked in all images. All scale bars are 20 μm.

**Variations in the pattern of IE protein expression in NSC.** Analysis of IE63 expression in 250 NSC revealed three major patterns. Most often, the NSC in acutely infected DRG showed expression of IE63 in both the nucleus of the neuron and the nuclei of the adjacent satellite cells within the same NSC (Fig. 1k; see also Fig. 1b and Fig. 2A). This pattern occurred in about 90% of infected NSC. Among the other infected NSC, one showed IE63 expression only in the neuron (Fig. 1i) and six had IE63 expression only in the satellite cells (Fig. 1j), indicating that neurons and satellite cells in the same NSC could become infected independently. Investigation of IE62 expression in NSC yielded similar results, as is evident in Fig. 1a and g and Fig. 4.

**Multiscale imaging of acutely infected DRG by correlative IF-EM.** The detection of IE, early and late viral proteins and VZV genomic DNA in satellite cells suggested that these cells, in addition to neurons, supported VZV replication in DRG in vivo. Correlative IF-EM makes it possible to relate immunohistological information about the presence of viral proteins or DNA in the complex microanatomy of neural tissue with ul-

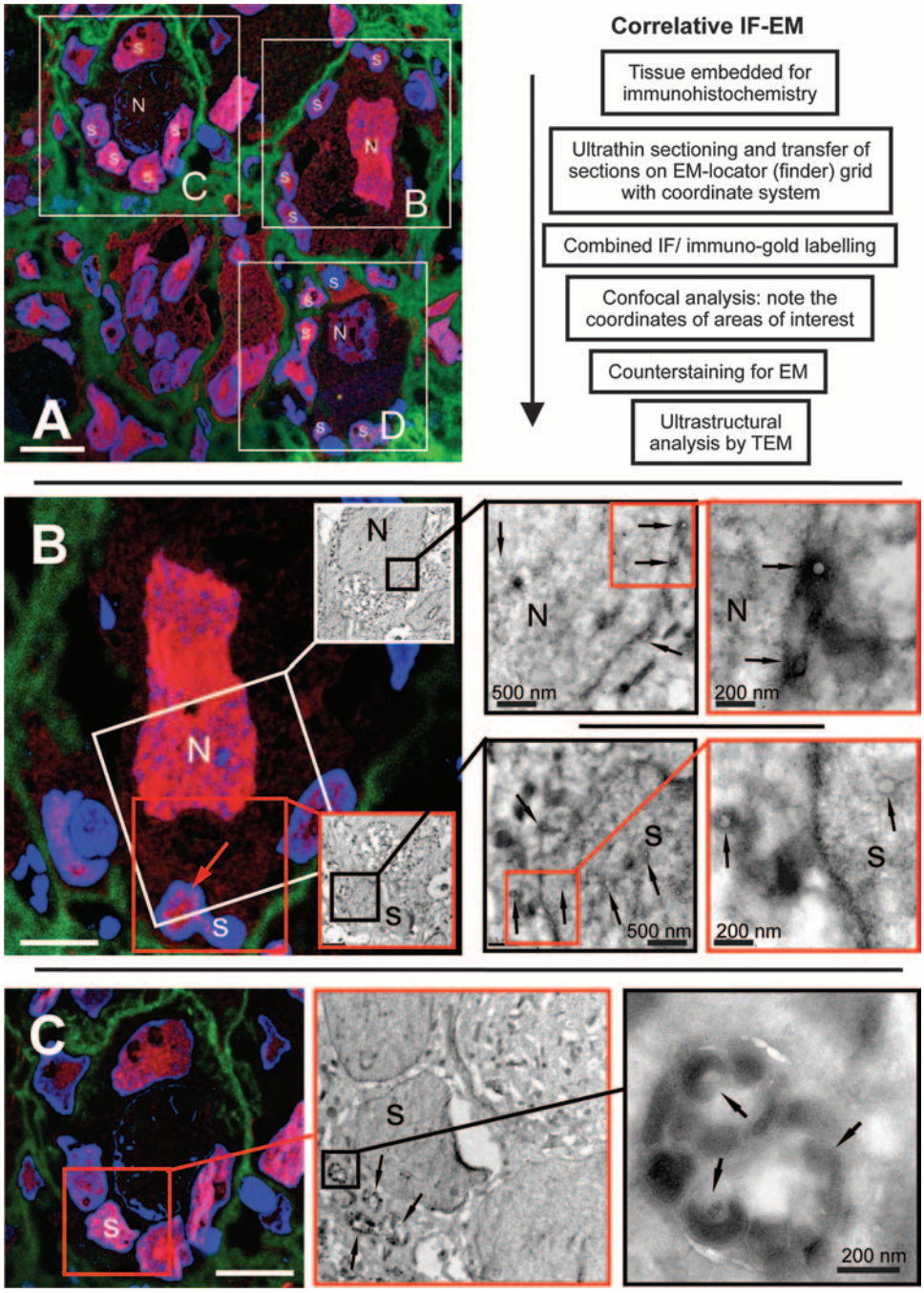


FIG. 2. Multiscale imaging of acutely infected DRG by correlative IF-EM. Ultrathin cryosections of acutely infected DRG were stained for IE63 (red) and collagen (green) (A to D). The primary antibody (anti-IE63) was detected with Texas red-labeled goat anti-rabbit antibody. Collagen was visualized with Alexa 488-labeled goat anti-mouse antibody. VZV genomic DNA was detected by DNA in situ hybridization of LR-White-embedded sections of acutely infected DRG using a DIG-labeled HindIII-C VZV DNA probe; hybridization was detected using mouse monoclonal anti-DIG antibody and Alexa 488-labeled rabbit anti-mouse antibody (E) or a protein A–15-nm colloidal gold conjugate (E and F). Nuclear DNA was counterstained with Hoechst 22358 (blue) (A to E). Identical areas imaged at increasing magnification are indicated by the linked squares with boundaries of the same color. Nuclei of neurons (N) and satellite cells (s) are marked in all images. (A) The white squares in the overview IF image enclose three NSC (NSC-B, NSC-C, NSC-D) in the same tissue section. These three NSC are analyzed further in panels B to D. Scale bar, 20 μm. An outline of the correlative IF-EM method is shown. (B) This panel demonstrates detection of nucleocapsids in IE63-expressing neuron and satellite cell nuclei. The IF image corresponds to the white square enclosing NSC-B in panel A, rotated by 180°. The white square in the IF image includes part of the nucleus of the neuron (N) that contains viral nucleocapsids, as shown at higher magnification in the TEM image of this area; sequential images at increasing magnification are provided in the linked black and red squares. Black arrows indicate nucleocapsids. The red square in the lower part of the IF image includes a satellite cell nucleus (s), indicated by a red arrow. The linked images of this area shown at increasing magnification demonstrate that this satellite cell contains viral nucleocapsids (black and red squares; black arrows). A cytoplasmic and tegumented nucleocapsid (left) and a nuclear nucleocapsid (right) are visible at high magnification (red square). Scale bars are 10 μm for IF or as indicated in nm for TEM. (C) This panel demonstrates enveloped VZV particles within cytoplasmic vacuoles in an

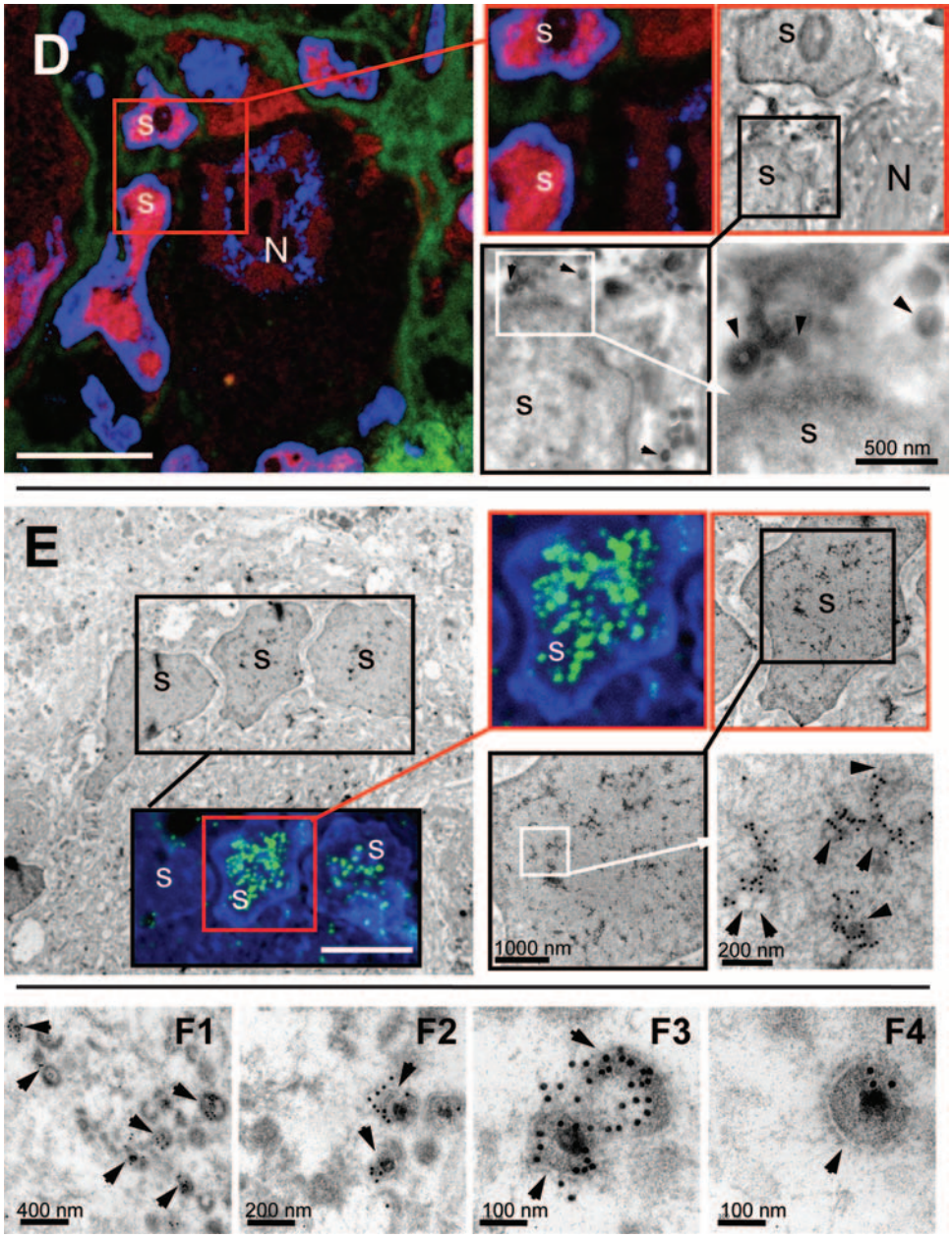


IE63-expressing satellite cell. The red square in the IF image includes an IE63-expressing satellite cell (s), shown at higher magnification in the EM image in the center. Numerous vacuoles harboring enveloped VZV particles (black arrows) are visible at increasing magnification of the area indicated by the black square, as shown in the image at the right. Scale bars are 15 μm for IF (left) or as indicated in nm for TEM. (D) This panel demonstrates extracellular VZV particles associated with the plasma membrane of IE63-expressing satellite cells. The red square in the IF image at the left includes the area between two IE63-expressing satellite cells (s). EM images of this area at increasing magnification are shown in the black and white squares. The black arrowheads indicate extracellular VZV particles at the plasma membrane of a satellite cell. Scale bars are 20 μm for IF (left) or as indicated in nm for TEM. (E) This panel demonstrates the ultrastructural localization of viral DNA in a satellite cell nucleus. The black square in the EM image at the left includes three satellite cell nuclei (s) that are also shown in the inset IF image. Viral DNA is detected by in situ hybridization using the VZV HindIII-C probe (green), and nuclei are stained with Hoechst (blue). TEM at increasing magnification using immunogold labeling to detect the VZV DNA probe is illustrated in the linked images shown in the black and white squares. This analysis reveals association of the viral DNA signal (15-nm gold particles) with VZV nucleocapsids (black arrowheads). Scale bars are 10 μm for IF (left) or as indicated in nm for TEM. (F) This panel demonstrates localization of viral genomic DNA to extracelluar VZ virions in DRG. VZV genomic DNA, detected as clusters of 15-nm gold particles, localizes specifically to VZ virions (arrowheads). No clusters are observed in the area surrounding the virions (F1 and F2). Clusters of from 3 to 20 gold particles are associated with the VZV genome within individual virions (F3 and F4). VZV DNA labeling is usually not restricted only to the nucleocapsid because efficient hybridization requires release of viral genomic DNA from the nucleocapids by proteinase K digestion and it is denatured and spread by alkaline treatment for efficient DNA hybridization to occur. Scale bars are as indicated in nm.

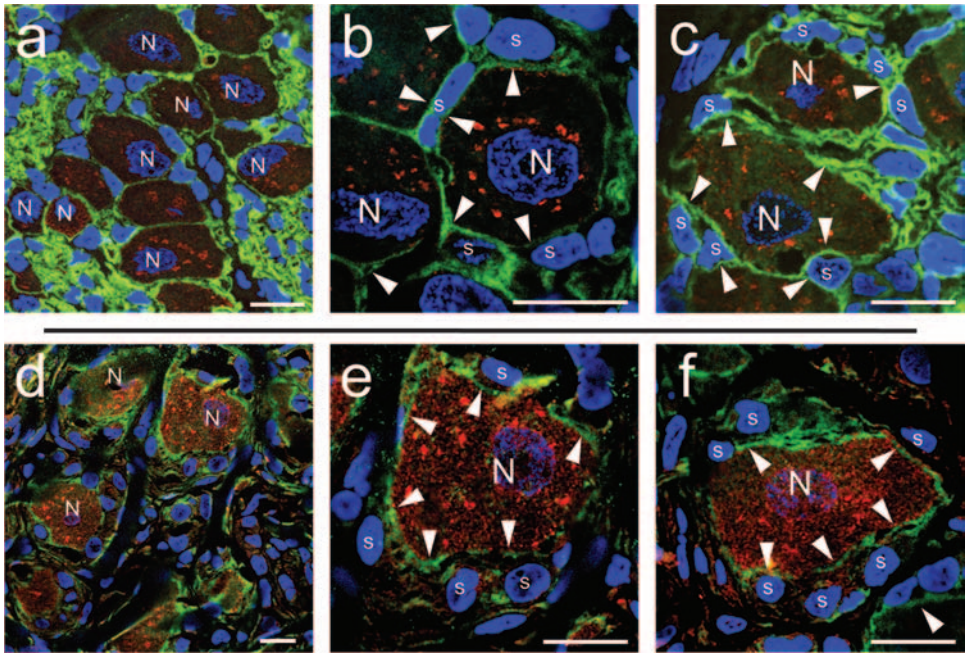


FIG. 3. Satellite cells and their associated neuron cell bodies within uninfected DRG are separated by cell membranes that express NCAM. Cryosections of either uninfected and unimplanted (a to c) or mock-infected and implanted DRG (d to f) were stained with mouse monoclonal anti-NCAM antibody (green), rabbit polyclonal anti-synaptophysin antibody (red), and Hoechst (blue). For secondary detection, Texas red-labeled goat anti-rabbit and or FITC-labeled goat anti-mouse antibodies were used. All images show the merge of the NCAM, synaptophysin, and nuclear DNA staining. Nuclei of neurons (N) and satellite cells (s) are marked. White arrowheads point to cell boundaries between neuron and satellite cells detected by NCAM staining (green). Scale bars, 20 μm.

trastructural details of virion assembly and cell structures (Fig. 2). This method was used to investigate whether VZV nucleocapsids were assembled in satellite cell nuclei and if enveloped virions were present in the cytoplasm of these cells and could be released to yield extracellular VZV particles. To identify infected NSC within DRG, ultrathin cryosections (80 nm) were prepared, transferred to an EM locator grid and stained for IE63 and with Hoechst stain to visualize the cell nuclei (Fig. 2A to D). Examination by confocal microscopy revealed IE63 expression in most NSC, as shown in the overview image in Fig. 2A. IE63 expression was observed in the nuclei of both neurons and satellite cells as described above (Fig. 1). Individual NSC were surrounded by collagen (Fig. 2A to D). Layers of collagen fibers that are known to enclose NSC were also demonstrated by TEM (not shown). Three individual NSC, designated NSC-B, NSC-C and NSC-D are shown within white squares in the overview image. These areas were examined at higher magnification and in combination with TEM, respectively, in Fig. 2B to D, as described below.

**VZV nucleocapsids are assembled in nuclei of neurons and satellite cells.** As expected, viral nucleocapsids could be readily identified in the nuclei of neurons that expressed IE63 using correlative IF-EM. The IF image in Fig. 2B (left panel) corresponds to NSC-B shown in the overview (Fig. 2A). The large nucleus of the neuron and several of the surrounding satellite cells of the same NSC unit strongly express IE63. High-resolution examination of the same section by TEM revealed several VZV nucleocapsids in the nucleus and cytoplasm of the infected neuron that were identified by IE63 expression; the TEM analysis shown at increasing magnifications is shown in the linked white, black, and red squares. VZV nucleocapsids were also observed in the nuclei of satellite cells that expressed IE63. For example, several intranuclear and cytoplasmic nucleocapsids were detected by TEM in the IE63-positive satellite cell indicated in the IF overview of the same NSC-B unit (Fig. 2B). Linked TEM images of this area show these nucleocapsids at increasing magnification.

**Intracellular enveloped virions are present in cytoplasmic vacuoles of satellite cells.** To further define the role of satellite cells in productive infection of DRG, correlative IF-EM was used to investigate more IE63-expressing satellite cells. TEM examination of several infected satellite cells revealed cytoplasmic vacuoles filled with enveloped and tegumented VZV particles within these cells. A representative example is presented in Fig. 2C. The IF image in Fig. 2C corresponds to NSC-C, marked by the white square in the overview IF in Fig. 2A. The red square in Fig. 2C surrounds one of several IE63-expressing satellite cells. The same satellite cell is presented at increasing magnification as visualized by TEM (Fig. 2C, center and right panels). Intracellular vacuoles filled with viral particles were clearly visible.

**Extracellular VZV particles were associated with plasma membranes of satellite cells.** Extracellular VZV particles were readily observed in the tissue spaces around both neurons and satellite cells by TEM. Correlative IF-EM allowed a targeted assessment of the area between two adjacent satellite cells that expressed IE63 (Fig. 2D) to determine whether extracellular virions were associated with the plasma membranes of these cells. The area of interest between the two satellite cells is marked by a red square in the IF images, which was then

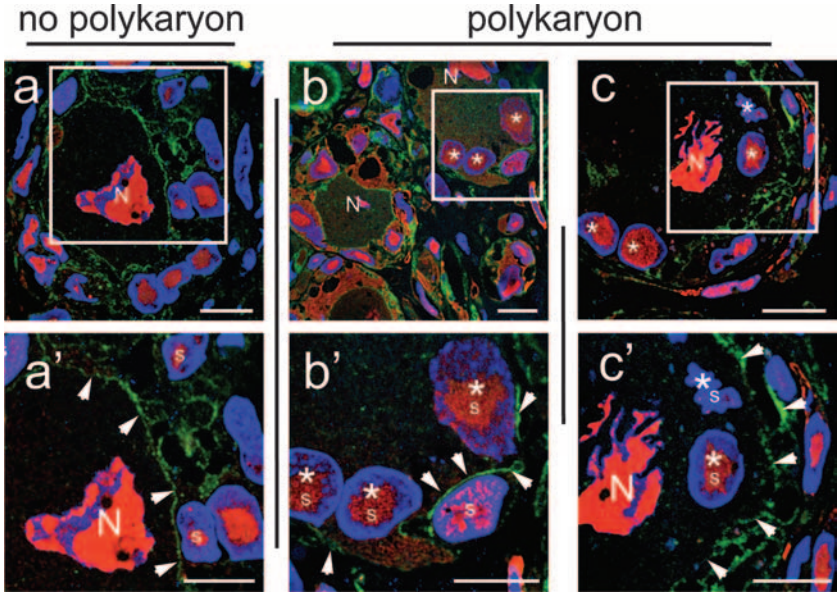


FIG. 4. Evidence for polykaryon formation in acutely infected DRG by immunofluorescence analysis. Cryosections of VZV-infected DRG were stained with mouse monoclonal anti-NCAM antibody (green), rabbit polyclonal anti-IE62 antibody (red) and Hoechst stain (blue). For secondary detection, Texas red-labeled goat anti-rabbit or FITC-labeled goat anti-mouse antibodies were used. All images show the merge of the NCAM (green), IE62 (red), and nuclear DNA staining (blue). Nuclei of neurons (N) and satellite cells (s) are marked. Additionally, nuclei of satellite cells located within a putative polykaryon are marked with an asterisk. White arrowheads point to cell boundaries detected by NCAM staining (green). The white squares in the overview images (a, b, and c) correspond to the area shown at higher magnification in the lower panels (a′, b′, and c′). Scale bars, 10 μm.

examined by TEM. Extracellular virions associated with the plasma membrane of a satellite cell were observed at the highest magnification (smaller panels at the right in Fig. 2D). The morphology of VZV particles appears somewhat different in these cryosections, which were counterstained only with uranyl acetate for TEM, compared to standard EM. In thawed cryosections, the nucleocapsid staining is generally less electron dense (Fig. 2B), the tegument is usually very electron dense (black), and most membranes appear white because they are not postfixed and stained with osmium tetroxide (Fig. 2C and D). The presence of numerous nucleocapsids and viral particles within satellite cells and associated with the cell membrane of satellite cells was confirmed by standard EM (see Fig. 5).

**VZV genomic DNA localizes to nucleocapsids in satellite cell nuclei.** The use of correlative IF-EM analysis of LR-White-embedded DRG in combination with VZV DNA in situ hybridization, made it possible to identify individual satellite cell nuclei harboring VZV genomic DNA by confocal microscopy and TEM on the same ultrathin section (Fig. 2E). This method allowed the correlation of the fluorescent VZV DNA signal with clusters of 15-nm gold particles that represent the VZV DNA signal at the ultrastructural level. Numerous clusters of 15-nm gold particles were closely associated with viral nucleocapsids that appeared as ring-like structures, as indicated in the highest-magnification image at the lower right in Fig. 2E. In an additional experiment, viral genomic DNA could be clearly localized to individual extracellular VZV particles (Fig. 2F1 to F4). The clusters of 15-nm gold particles were associated with virions, were completely absent from the surrounding extracellular matrix (Fig. 2F1 and F2), and were not observed in uninfected cells (not shown). Clusters of 3 to 20 gold particles were associated with a single extracellular virion. Since each virion contains only one genome, the in situ hybridization method was sensitive enough to identify a single VZV genome copy.

**Evidence for polykaryon formation between VZV-infected neurons and satellite cells.** The evaluations of the expression of IE62 and IE63 in some NSC revealed a homogeneous staining of the cytoplasm of the neuron and the surrounding satellite cells, and no cell membranes separating the two cell types were evident. The NSC stained with IE63 in Fig. 1b exemplifies this observation. Because cell-cell fusion with resulting polykaryon formation is a hallmark of VZV infection in VZV skin lesions and in cultured cells, we hypothesized that an infected neuron and satellite cells within an individual NSC might fuse to form a polykaryon in acutely infected DRG. To test this hypothesis, we first performed extensive experiments using 500-nm cryosections of human fetal DRG that were not infected or implanted in SCID mice (Fig. 3a to c) and of mock-infected DRG xenografts (Fig. 3d to f) that were otherwise treated in the same way as VZV-infected DRG. The control DRG were stained with a polyclonal rabbit antibody specific for synaptophysin, which is expressed in cytoplasmic vesicles in the neuron and with a mouse monoclonal antibody specific for NCAM, which is expressed on membranes of neurons and satellite cells in the NSC (Fig. 3a to f). Satellite cells adjacent to a neuron were always separated from the neuronal cell cytoplasm by NCAM-stained cell membranes. Satellite cells have limited cytoplasm. In areas where these cells are densely packed and imaged at lower magnification, NCAM staining may appear cytoplasmic (Fig. 3a); however, at higher magnification, membrane restriction of NCAM is evident (Fig. 3b

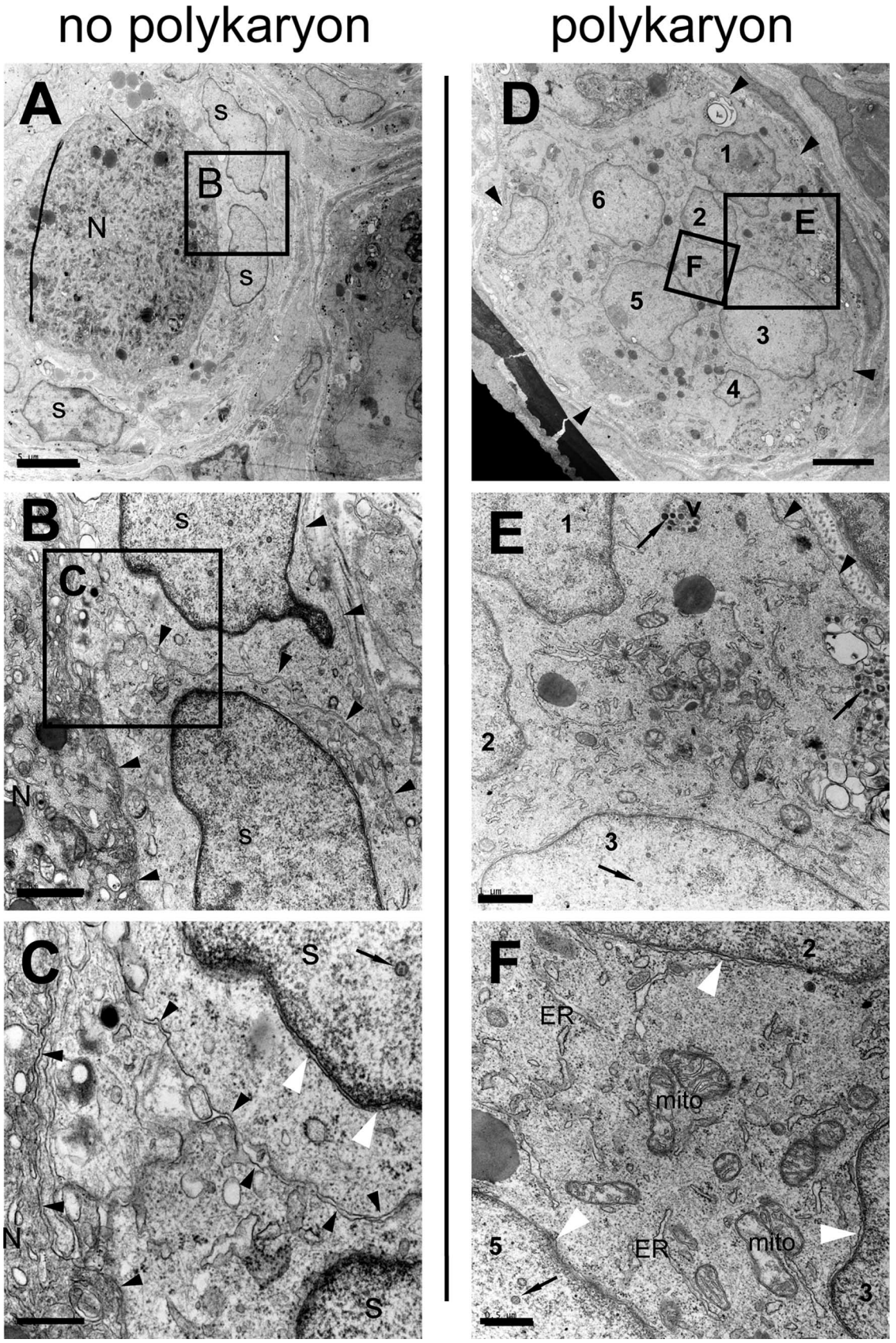


FIG. 5. Ultrastructural analysis of NSC in acutely infected DRG. Acutely infected DRG were fixed and embedded for standard EM. Ultrathin sections were counterstained with lead citrate and uranyl acetate and investigated by TEM. The NSC shown in panels A to C or D to F, respectively,

and c). In Fig. 3, the white arrowheads indicate NCAM-stained cell boundaries (green) separating the neuron from the adjacent satellite cells. When 50 NSC in the unimplanted DRG control tissues were evaluated, none of the satellite cells showed any evidence of polykaryon formation with the neuron. Furthermore, 108 NSC in the mock-infected/implanted DRG control tissues were evaluated and none of 679 satellite cells within these NSC showed cell-cell fusion with the neuron. NCAM and synaptophysin expression did not differ between unimplanted/uninfected (Fig. 3a to c) and implanted/mock-infected DRGs (Fig. 3d to f).

When patterns of NCAM expression had been established in uninfected human DRGs, VZV-infected DRG were examined for NCAM and IE62 expression in 500-nm cryosections (Fig. 4). The evaluation of 252 NSC in acutely infected DRG demonstrated that up to 50% (123/252) of the complexes showed evidence of polykaryon formation at day 14 after infection, based on the criteria of the absence of NCAM-expressing membranes between the neuronal cell body and the adjacent satellite cells and a homogeneous intensity of cytoplasmic IE62 expression. Representative examples are shown in Fig. 4; the white square in the overview image is shown at higher magnification in Fig. 4a′. The left panels, which are labeled "no polykaryon," show an example of an NSC with an obvious NCAM-expressing membrane that separates the neuronal cell body from the adjacent satellite cells (Fig. 4a′). Both the neuron nucleus and the satellite cells in this NSC express IE62. These experiments also suggest that NCAM continues to be expressed and is not substantially down-regulated by VZV infection.

In contrast, the panels labeled "polykaryon" show NSC that contain satellite cells that express nuclear IE62 and have no apparent separation from the neuronal cell body by an NCAM-expressing cell membrane (Fig. 4b, b′, c, and c′). This pattern suggests fusion between plasma membranes of adjacent satellite cells and the neuronal plasma membrane. The higher magnification of the NSC in Fig. 4b′ reveals a small area of NCAM expression which is located between one of the satellite cells and the neuronal cell body, whereas there is no NCAM-expressing membrane visible between the three other satellite cell nuclei and the same neuron cell body. However, NCAM expression was present on the cell membrane that encloses both the neuron and the satellite cells with which it is fused (Fig. 4b′). Another example of satellite cell nuclei that had no separation from the neuronal cell body by an NCAM-expressing plasma membrane is shown in Fig. 4c and c′. The higher magnification in Fig. 4c′ confirms the loss of the plasma membrane between the large neuron nucleus and the two adjacent smaller satellite cell nuclei; however, these nuclei are surrounded by an outer NCAM-expressing membrane (Fig. 4c′).

**Ultrastructural evidence for polykaryon formation.** In these experiments, acutely infected DRG were embedded in epoxy resin for standard EM and ultrathin sections were evaluated by TEM (Fig. 5). As was suggested by confocal microscopy analysis of the NSC shown in Fig. 4a and a′, some infected NSC were identified in which no fusion of the neuronal cell body with the adjacent satellite cells had occurred. The series of TEM images at increasing magnification in Fig. 5A, B, and C illustrate this observation. In this case, the plasma membranes of both the satellite cells and the neuron were clearly identifiable. These images demonstrate the good preservation of cell membranes under these conditions and show that a double-membrane-like structure results when two DRG cells, each surrounded by its own plasma membrane, are adjacent, as is evident at the site of contact between two satellite cells or between the satellite cell and the neuronal cell body, as indicated in Fig. 5B and C.

However, numerous examples of polykaryon formation in NSC were readily detected by ultrastructural analyses of acutely infected DRG. The representative examples of polykaryons, presented in Fig. 5D to F and Fig. 6A to C, were identified on the same EM grid and therefore had been exposed to identical staining conditions as the NSC shown in Fig. 5A to C. The polykaryon shown in Fig. 5D to F harbors at least six nuclei within the cytoplasm, and the polykaryon shown in Fig. 6A to C contains at least four nuclei. No plasma membranes separating these nuclei could be identified at higher magnification of the area between the nuclei (see Fig. 5E and F or Fig. 6B and C), indicating that they share the same cytoplasm and are therefore part of a polykaryon. Nevertheless, even when cell membranes between neuron and satellite cell nuclei were absent, a continuous cell membrane persisted around the margins of the polykaryon (Fig. 5D and E or Fig. 6B). Evidence of productive viral replication within these polykaryons was provided by the detection of VZV nucleocapsids (in nuclei 3 and 5 at the lower edges of Fig. 5E and F, respectively, or in Fig. 6C), intracellular viral particles in a cytoplasmic vacuole (Fig. 5E), and numerous extracellular virions adjacent to the cell membrane of the polykaryon (Fig. 5E). Despite productive infection, the membranes of the nuclei within these and other polykaryons appeared morphologically intact (Fig. 5F and Fig. 6C) and the mitochondria and the endoplasmic reticulum did not show obvious morphological damage (best seen in Fig. 5F). However, some other neurons and satellite cells in VZV-infected DRG showed extensive cytopathic effects (Fig. 6D to F). The nuclei of these cells

were found on the same EM grid. Black arrowheads point to the cell membrane surrounding satellite cells or the neuron cell body (B and C) or a polykaryon (D and E). In panels A to C, the nuclei of satellite cells are marked "s" and the neuronal cell body is marked "N." The nuclei within the polykaryon shown in panels D and E are numbered 1 to 6. Thin black arrows point to VZV nucleocapsids (nucleus 3 in panel E and nucleus 5 in panel F), intracellular virions (at the top in panel E), or extracellular virions (at the right side in panel E). The white arrowheads in panel F point to the nuclear envelope of three different nuclei within the polykaryon. The endoplasmic reticulum (ER) and mitochondria (mito) are marked in panel F. Black boxes labeled B, C, E, and F indicate the area that is seen at higher magnification in the images in panel B, C, D, and F, respectively. Despite the normal morphology of the nuclear envelope, mitochondria, and the ER in the polykaryon (F), no cell membranes can be detected between the nuclei of the polykaryon, as is evident by comparing panels E and F with panels B and C. Scale bars are 5 μm for panels A and D, 1 μm for panels B and E, or 0.5 μm for panels C and F.

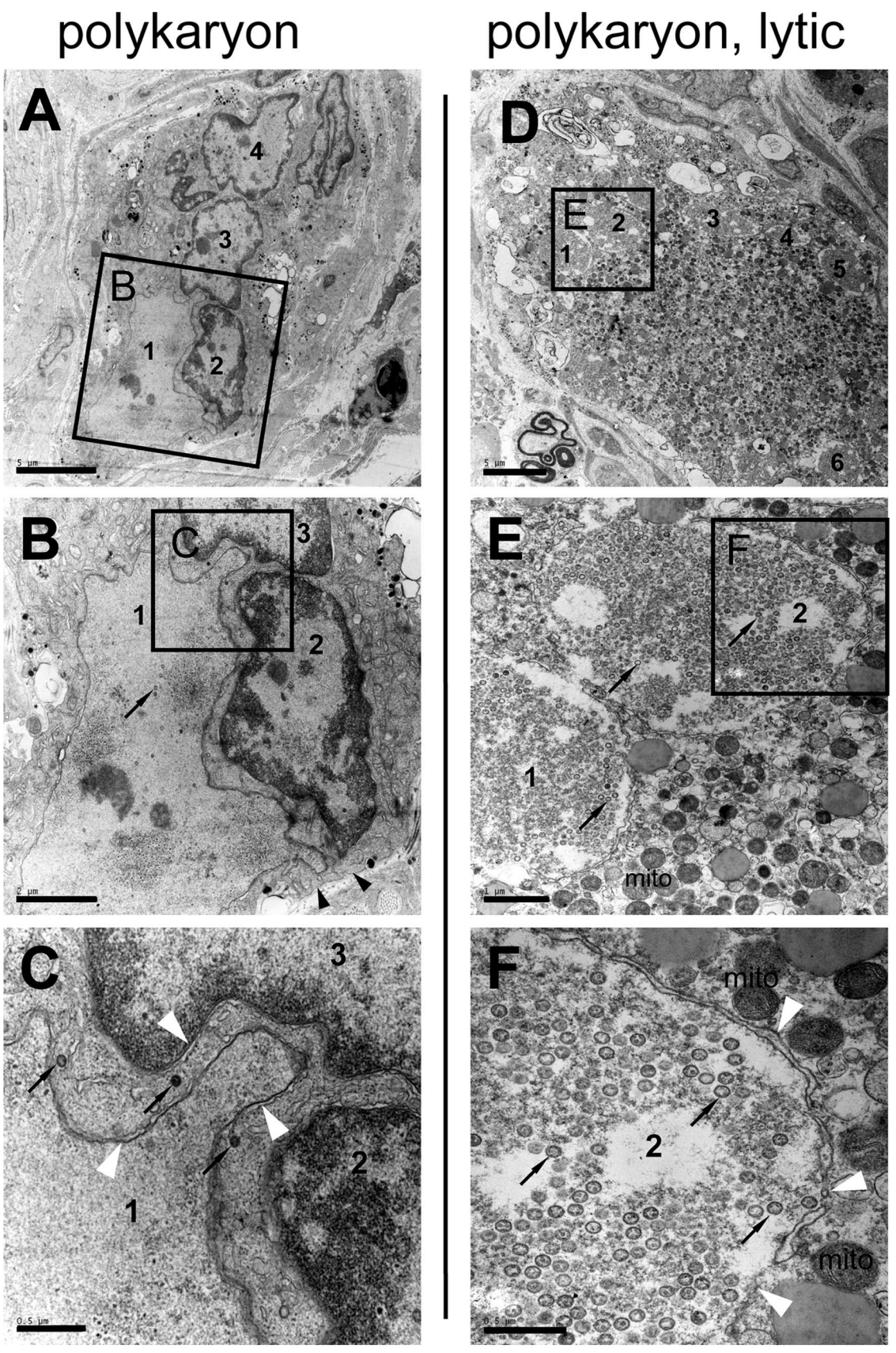


FIG. 6. Ultrastructural analysis of NSC in acutely infected DRG showing lytic infection. Panels A to F show a different area of the same EM grid presented in Fig. 5. Black arrowheads point to the cell membrane surrounding a polykaryon (B). The nuclei of the polykaryons are numbered

contained masses of viral nucleocapids, nuclear envelopes had disintegrated, intracellular membranes were difficult to recognize, and mitochondria were electron dense and swollen.

## DISCUSSION

In this study, the cellular tropisms of VZV and mechanisms of VZV neuropathogenesis during acute infection of human DRG xenografts in the SCIDhu mouse model were examined by correlative IF-EM (35, 36). This approach allowed the analysis of viral protein expression, VZV genomic DNA synthesis, virion assembly and cellular changes at both the histological and the ultrastructural level in the same cell. Our experiments support a role for satellite cells as well as neurons in VZV infection in human DRG in the SCIDhu mouse model. We also demonstrated that VZV has the capacity to cause fusion of the plasma membranes of these two distinct types of differentiated cells that form the characteristic NSC within the sensory ganglia of the peripheral nervous system. These observations provide a better understanding of neuropathogenic mechanisms in acute VZV infection of sensory ganglia and help to explain the neuropathologic consequences of active VZV replication in human sensory ganglia that are associated with clinical episodes of herpes zoster.

VZV proteins, including IE proteins, IE62 and IE63, the early ORF47 kinase protein and the late glycoprotein, gE, were expressed in the majority of satellite cells as well as neurons in VZV-infected DRG xenografts. Viral genomic DNA was detected in nuclei of infected neurons and satellite cells that had been identified by IE63 protein expression. Viral proteins were also expressed by both neurons and nonneuronal cells in cultured human DRG infected with VZV in vitro (13). Productive VZV infection requires nucleocapsid assembly, nuclear egress, viral envelopment, and release of infectious virions. Satellite cells as well as neurons contained intranuclear and cytoplasmic nucelocapsids and intracelluar enveloped virions within cytoplasmic vacuoles and VZV particles were located external to the plasma membranes of both cell types. Although EM cannot establish that these particles are infectious, nucleocapsids and VZV particles in satellite cells had no apparent ultrastructural differences from those in neurons. Given that each neuron is surrounded by several satellite cells, the quantity of VZ virions produced by satellite cells may exceed that of neurons in acutely infected DRG. Virions were also present in the nuclei and cytoplasm of many satellite cells in the EM analysis of a trigeminal ganglion recovered at autopsy from a patient who developed zoster 4 days before death (8). Furthermore, although neurons appear to be the primary site of VZV persistence in sensory ganglia, VZV genomes may also be maintained after infection of some satellite cells (19, 28, 34).

During herpes zoster, neuronal cell bodies must be infected in order for the virus to gain access to peripheral nerve axons for transport to skin. However, since at most about 5% of neurons in sensory ganglia appear to be latently infected (19, 28), transfer of VZV into other neurons would substantially enhance VZV access to skin. In these experiments, some NSC were observed in acutely infected DRG xenografts in which only satellite cells contained VZV DNA or expressed VZV proteins and appear to have been infected independently of the associated neuron cell body. In addition, infected satellite cells released VZ virions. Amplification of VZV reactivation by replication in satellite cells, followed by virion entry into previously uninfected neurons is consistent with the widespread ganglionitis observed in ganglia obtained at autopsy from patients with herpes zoster (8, 12, 14, 23). A process of VZV transfer into satellite cells, leading to infection of their associated neuronal cell bodies, may also account for the gradual emergence of new clusters of skin lesions in the involved cutaneous dermatome during episodes of herpes zoster. Direct VZV infection of satellite cells could also occur during primary VZV infection when the virus may gain access to sensory ganglia by a hematogenous route through VZV infection of T cells, enhancing the capacity of the virus to establish latency (4, 35).

Our experiments also suggest that polykaryon formation between satellite cells and neurons is a mechanism of potential importance in the neurobiology of VZV infection in sensory ganglia. Fusion with adjacent cells and formation of syncytia are characteristic of VZV infection in cultured cells in vitro and between epidermal cells in the skin lesions that are formed during varicella or herpes zoster. This process requires the expression of viral glycoproteins on plasma membranes of infected cells, which then undergo fusion with neighboring uninfected cells (6). The unique observation in VZV-infected DRG xenografts was that VZV-induced cell fusion was demonstrated between satellite cells and neurons, which are two fully differentiated, distinct cell types within sensory ganglia (15). In uninfected human DRG, neuronal cell bodies and the surrounding satellite cells were separated by an NCAM-expressing membrane. In contrast, high-resolution images of VZV-infected DRG showed diffuse, homogeneous IE62 and IE63 expression and the absence of NCAM-expressing plasma membranes between satellite cells and neurons. This loss of the plasma membrane between the neuronal cell body and adjacent satellite cells was associated with preservation of an NCAM-positive plasma membrane surrounding the cytoplasmic compartment that contained the neuronal cell body and satellite cell nuclei.

Ultrastructural analysis provided definitive evidence of polykaryon formation between neurons and adjacent satellite cells in infected NSC. In NSC that did not have polykaryon formation by IF analysis, high-magnification EM imaging showed

(A to F). Thin black arrows point to VZV nucleocapsids (B, C, E, and F). The white arrowheads in panels C and F point to the nuclear envelopes of different nuclei within the polykaryon. The mitochondria (mito) are marked in panels E and F. Black boxes labeled B, C, E, and F indicate the area that is seen at higher magnification in the images in panel B, C, D, and F, respectively. No cell membranes can be detected between the nuclei of the shown polykaryons (A to C or D to F). The polykaryon in panels D to F contains nuclei that are massively filled with viral nucleocapsids (black arrows) and shows cytopathic alterations, including dense mitochondria and disintegrating nuclear envelopes (F). Scale bars are 5 μm for panels A and D, 2 μm for panel B, 1 μm for panel E, or 0.5 μm for panels C and F.

two separate membranes lying in very close proximity to each other between adjacent neuron and satellite cells. In NSC that had formed a polykaryon by IF analysis, no cell membranes could be detected and the nuclei of the neuron and satellite cells were located in a common cytoplasm. Importantly, most of these polykaryons did not show any obvious damage of the nuclear envelope or intracellular organelles, despite the presence of many nucleocapsids and enveloped virions in the cytoplasm. Preservation of these structures is presumed to be critical for the life cycle of herpesviruses in infected cells (30). The extensive expression of the IE63 protein is of interest in this regard since it has been shown to be important for inhibiting apoptosis of VZV-infected primary neurons in vitro, based on reduced inhibition of apoptosis by a VZV mutant that had only one copy of the duplicated gene (17, 18). These experiments indicated that merging of the satellite and neuronal cell cytoplasm occurs during active VZV replication in NSC and was not a late effect attributable to cellular necrosis in VZV-infected sensory ganglia. Incomplete boundaries between neurons and satellite cells were also noted in the ultrastructural examination of a VZV-infected trigeminal ganglion obtained at autopsy (8).

Taken together, these observations suggest a model in which VZV replication in a single neuron, resulting in polykaryon formation with adjacent satellite cells, is the first event in the acute infection of sensory ganglia caused by VZV reactivation from latency. VZ virions released from these satellite cells can then infect nearby satellite cells that surround other neuronal cell bodies. Polykaron formation between these secondarily infected satellite cells and their neuronal cell bodies would then enhance access of VZ virions to neuronal axons for transport to skin sites of replication. This model predicts that most neurons become infected by VZ virions that are released into the DRG by productively infected satellite cells, rather than by the simultaneous reactivation of latent VZV genomes harbored by multiple neurons within the affected ganglion. VZV gE, like its HSV homologue, appears to play a critical role in cell-cell fusion and its heterodimer partner, gI, contributes to this gE function (2, 9, 18, 24, 29, 30). As would be expected from this model, infection with a VZV mutant that lacked gI resulted in highly restricted VZV replication in SCIDhu DRG xenografts (36). Recent studies also indicate that neurons in sensory ganglia have microvilli that extend into invaginations of satellite cells and that functional gap junctions exist between the neuronal cell body and its satellite cells (16, 25–27). These characteristics have the potential to facilitate cell-cell fusion mediated by VZV proteins and enhance viral spread between neuronal cell bodies and satellite cells. It is also of interest that VZV exhibits little tropism for cells in the central nervous system and very rarely causes encephalitis (12). Although information about satellite cells in sensory ganglia is limited compared to what is known about peripheral neurons, these cells appear to have both similarities and differences when compared to glial cells in the central nervous system (15, 26). Whether VZV tropism for satellite cells within sensory ganglia reflects some underlying differences between these glial cell subtypes warrants further study.

Recruitment of antiviral T cells into the VZV-infected ganglion is presumed to control acute viral replication over time, although anti-VZV T cells do not appear to be persistent in latently infected ganglia (33). The neuropathology produced by satellite cell infection and polykaryon formation during VZV neuropathogenesis in sensory ganglia would be predicted to occur at an early stage of VZV reactivation, and repair of the damage would be expected to be a prolonged process. These observations about VZV infection in the SCIDhu DRG model should be extended by examining autopsy DRG from patients with herpes zoster at the time of death in order to further explore the role of cell-cell fusion and satellite cell infection in the clinical context. Clinically, the amplification and efficient spread of VZV within DRG by these mechanisms help to explain the significant risk of prolonged neurologic signs and symptoms associated with herpes zoster (12).

## ACKNOWLEDGMENTS

This work was supported by NIH grants (AI053846, AI20459, and CA049605) to A.M.A. and by a postdoctoral fellowship to M.R. from the Deutsche Forschungsgemeinschaft, DFG, Germany (Geschaeftszeichen: RE2716/1-1).

Sample preparation, sectioning, and IF-EM-analysis were performed in the CSIF/Stanford University Medical School.

## REFERENCES

1. **Ako-Adjei, D., M. C. Johnson, and V. M. Vogt.** 2005. The retroviral capsid domain dictates virion size, morphology, and coassembly of Gag into virus-like particles. J. Virol. **79:**13463–13472.
2. **Berarducci, B., M. Ikoma, S. Stamatis, M. Sommer, C. Grose, and A. M. Arvin.** 2006. Essential functions of the unique N-terminal region of the varicella-zoster virus glycoprotein E ectodomain in viral replication and in the pathogenesis of skin infection. J. Virol. **80:**9481–9496.
3. **Besser, J., M. H. Sommer, L. Zerboni, C. P. Bagowski, H. Ito, J. Moffat, C.-C. Ku, and A. M. Arvin.** 2003. Differentiation of varicella-zoster virus ORF47 protein kinase and IE62 protein binding domains and their contributions to replication in human skin xenografts in the SCID-hu mouse. J. Virol. **77:** 5964–5974.
4. **Cohen, J., S. Straus, and A. Arvin (ed.).** 2007. Varicella-zoster virus replication, pathogenesis, and management, 5th ed., vol. 2. Lippincott-Williams & Wilkins, Philadelphia, PA.
5. **Cohrs, R. J., and D. H. Gilden.** 2007. Prevalence and abundance of latently transcribed varicella-zoster virus genes in human ganglia. J. Virol. **81:**2950–2956.
6. **Cole, N. L., and C. Grose.** 2003. Membrane fusion mediated by herpesvirus glycoproteins: the paradigm of varicella-zoster virus. Rev. Med. Virol. **13:** 207–222.
7. **Darcy, K. J., K. Staras, L. M. Collinson, and Y. Goda.** 2006. Constitutive sharing of recycling synaptic vesicles between presynaptic boutons. Nat. Neurosci. **9:**315–321.
8. **Esiri, M. M., and A. H. Tomlinson.** 1972. Herpes zoster. Demonstration of virus in trigeminal nerve and ganglion by immunofluorescence and electron microscopy. J. Neurol. Sci. **15:**35–48.
9. **Farnsworth, A., and D. C. Johnson.** 2006. Herpes simplex virus gE/gI must accumulate in the *trans*-Golgi network at early times and then redistribute to cell junctions to promote cell-cell spread. J. Virol. **80:**3167–3179.
10. **Giannone, G., B. J. Dubin-Thaler, O. Rossier, Y. Cai, O. Chaga, G. Jiang, W. Beaver, H. G. Dobereiner, Y. Freund, G. Borisy, and M. P. Sheetz.** 2007. Lamellipodial actin mechanically links myosin activity with adhesion-site formation. Cell **128:**561–575.
11. **Giepmans, B. N., T. J. Deerinck, B. L. Smarr, Y. Z. Jones, and M. H. Ellisman.** 2005. Correlated light and electron microscopic imaging of multiple endogenous proteins using Quantum dots. Nat. Methods **2:**743–749.
12. **Gilden, D., R. Mahalingam, S. Deitch, and R. Cohrs (ed.).** 2006. Varicella-zoster virus neuropathogenesis and latency. Caister Academic Press, Norwich, United Kingdom.
13. **Gowrishankar, K., B. Slobedman, A. L. Cunningham, M. Miranda-Saksena, R. A. Boadle, and A. Abendroth.** 2007. Productive varicella-zoster virus infection of cultured intact human ganglia. J. Virol. **81:**6752–6756.
14. **Greenfield, J. G. A., and J. Hume.** 1992. Greenfield's neuropathology, 5th ed. Oxford University Press, New York, NY.
15. **Hanani, M.** 2005. Satellite glial cells in sensory ganglia: from form to function. Brain Res. Rev. **48:**457–476.
16. **Hanani, M., T. Y. Huang, P. S. Cherkas, M. Ledda, and E. Pannese.** 2002. Glial cell plasticity in sensory ganglia induced by nerve damage. Neuroscience **114:**279–283.
17. **Hood, C., A. L. Cunningham, B. Slobedman, A. M. Arvin, M. H. Sommer, P. R. Kinchington, and A. Abendroth.** 2006. Varicella-zoster virus ORF63 inhibits apoptosis of primary human neurons. J. Virol. **80:**1025–1031.

18. **Hood, C., A. L. Cunningham, B. Slobedman, R. A. Boadle, and A. Abendroth.** 2003. Varicella-zoster virus-infected human sensory neurons are resistant to apoptosis, yet human foreskin fibroblasts are susceptible: evidence for a cell-type-specific apoptotic response. J. Virol. **77:**12852–12864.
19. **Levin, M. J., G.-Y. Cai, M. D. Manchak, and L. I. Pfizer.** 2003. Varicella-zoster virus DNA in cells isolated from human trigeminal ganglia. J. Virol. **77:**6979–6987.
20. **Lungu, O., C. A. Panagiotidis, P. W. Annunziato, A. A. Gershon, and S. J. Silverstein.** 1998. Aberrant intracellular localization of Varicella-Zoster virus regulatory proteins during latency. Proc. Natl. Acad. Sci. USA **95:**7080–7085.
21. **Miller, S. E., R. M. Levenson, C. Aldridge, S. Hester, D. J. Kenan, and D. N. Howell.** 1997. Identification of focal viral infections by confocal microscopy for subsequent ultrastructural analysis. Ultrastruct. Pathol. **21:**183–193.
22. **Mironov, A. A., A. A. Mironov, Jr., G. V. Beznoussenko, A. Trucco, P. Lupetti, J. D. Smith, W. J. Geerts, A. J. Koster, K. N. Burger, M. E. Martone, T. J. Deerinck, M. H. Ellisman, and A. Luini.** 2003. ER-to-Golgi carriers arise through direct en bloc protrusion and multistage maturation of specialized ER exit domains. Dev. Cell **5:**583–594.
23. **Okazaki, H.** 1983. Fundamentals of neuropathology, 1st ed. Igaku-Shoin, New York, NY.
24. **Olson, J. K., and C. Grose.** 1998. Complex formation facilitates endocytosis of the varicella-zoster virus gE:gI Fc receptor. J. Virol. **72:**1542–1551.
25. **Pannese, E.** 2002. Perikaryal surface specializations of neurons in sensory ganglia. Int. Rev. Cytol **220:**1–34.
26. **Pannese, E.** 1981. The satellite cells of the sensory ganglia. Adv. Anat. Embryol. Cell Biol. **65:**1–111.
27. **Pannese, E., M. Ledda, P. S. Cherkas, T. Y. Huang, and M. Hanani.** 2003. Satellite cell reactions to axon injury of sensory ganglion neurons: increase in number of gap junctions and formation of bridges connecting previously separate perineuronal sheaths. Anat. Embryol. (Berlin) **206:**337–347.
28. **Pevenstein, S. R., R. K. Williams, D. McChesney, E. K. Mont, J. E. Smialek, and S. E. Straus.** 1999. Quantitation of latent varicella-zoster virus and herpes simplex virus genomes in human trigeminal ganglia. J. Virol. **73:**10514–10518.
29. **Polcicova, K., K. Goldsmith, B. L. Rainish, T. W. Wisner, and D. C. Johnson.** 2005. The extracellular domain of herpes simplex virus gE is indispensable for efficient cell-to-cell spread: evidence for gE/gI receptors. J. Virol. **79:**11990–12001.
30. **Roizman, B., D. M. Knipe, and R. Whitley (ed.).** 2007. Herpes simplex viruses 5th ed., vol. 2. Lippincott-Williams & Wilkins, Philadelphia, PA.
31. **Somekh, E., D. G. Tedder, A. Vafai, J. G. Assouline, S. E. Straus, C. L. Wilcox, and M. J. Levin.** 1992. Latency in vitro of varicella-zoster virus in cells derived from human fetal dorsal root ganglia. Pediatr. Res. **32:**699–703.
32. **Takizawa, T., and J. M. Robinson.** 2006. Correlative microscopy of ultrathin cryosections in placental research. Methods Mol. Med. **121:**351–369.
33. **Verjans, G. M., R. Q. Hintzen, J. M. van Dun, A. Poot, J. C. Milikan, J. D. Laman, A. W. Langerak, P. R. Kinchington, and A. D. Osterhaus.** 2007. Selective retention of herpes simplex virus-specific T cells in latently infected human trigeminal ganglia. Proc. Natl. Acad. Sci. USA **104:**3496–3501.
34. **Wang, K., T. Y. Lau, M. Morales, E. K. Mont, and S. E. Straus.** 2005. Laser-capture microdissection: refining estimates of the quantity and distribution of latent herpes simplex virus 1 and varicella-zoster virus DNA in human trigeminal ganglia at the single-cell level. J. Virol. **79:**14079–14087.
35. **Zerboni, L., C. C. Ku, C. D. Jones, J. L. Zehnder, and A. M. Arvin.** 2005. Varicella-zoster virus infection of human dorsal root ganglia in vivo. Proc. Natl. Acad. Sci. USA **102:**6490–6495.
36. **Zerboni, L., M. Reichelt, C. D. Jones, J. L. Zehnder, H. Ito, and A. M. Arvin.** 2007. Aberrant infection and persistence of varicella-zoster virus in human dorsal root ganglia in vivo in the absence of glycoprotein I. Proc. Natl. Acad. Sci. USA **104:**14086–14091.